NONDESTRUCTIVE EVALUATION OF CONCRETE SPECIMENS REPRESENTATIVE OF NUCLEAR POWER PLANTS CONTAINING KNOWN DEFECTS

N. Dianne Bull Ezell*, Austin Albright, Dan Floyd, and Lev Khazanovich†

*Oak Ridge National Laboratory, 1 Bethel Valley Rd., Oak Ridge, TN 37831, bullnd@ornl.gov
†University of Pittsburgh, 4200 Fifth Ave, Pittsburgh, PA 15260

Many known defects that develop in concrete over time may threaten the safety and security of the infrastructure in nuclear power plants (NPPs). These defects also exist in other concrete infrastructures, but the harsher nuclear environment adds significant difficulty to their detection and correction. To monitor the structural health of a concrete facility, coring and other destructive testing methods are typically employed, but this is not the ideal solution for NPP concrete infrastructure. Developing a reliable nondestructive evaluation (NDE) method to evaluate the damage in these structures will greatly improve the long-term operation and safety of NPPs. The University of Tennessee, in collaboration with Oak Ridge National Laboratory, developed a large-scale experiment to study one known defect due to the reaction between hydroxyl ions of the alkalis in cement paste and the siliceous minerals present in some aggregates known as alkali-silica reactions (ASRs). *Alkali-silica gel forms and swells due to its hygroscopic characteristic, causing cracking and material failure. This paper discusses the NDE measurements performed on the large concrete specimens and the reconstructed images from these measurements.*

I. DEVELOPING A LARGE-SCALE EXPERIMENT

In 2010, the US Nuclear Regulatory Commission (NRC) reported that ASR was discovered in the Seabrook NPP concrete infrastructure [1]. As a result of this discovery, the NRC and the US Department of Energy (DOE) launched an investigation into the impact of ASR development. A large-scale experiment was fabricated at the University of Tennessee [2] that was representative of the infrastructure found in an NPP. Three rebar-reinforced specimens (3 m × 3.5 m × 1 m) were fabricated using two concrete mixtures: the unconfined control specimen (CTRL) used a concrete mixture known for not developing ASR, and the unconfined ASR (UASR) and confined ASR(CASR) used a concrete mixture that guaranteed ASR development (Figure 1). A large steel frame was placed around the CASR specimen to significantly limit expansion in the x and y axis, while the unconfined specimens were allowed to expand in all directions.

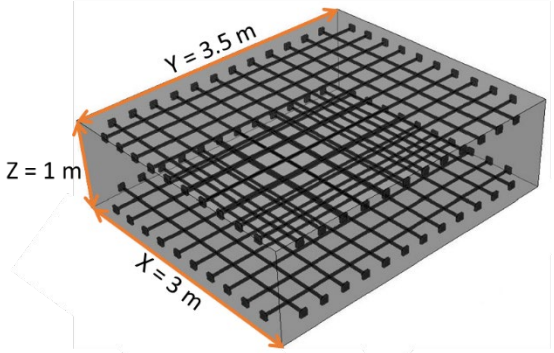

Fig. 1. Large, reinforced concrete specimen.

Since ASR requires a long period of time to develop, the experiment was housed in a 16,000 ft^3 environmental chamber that was held at 38°C (100°F) with 95% relative humidity to ensure a 0.5% expansion in the concrete over a two-year period. However, the accelerated expansion developed faster than anticipated in the first year, so the temperature was dropped to 21°C (70°F) while maintaining a 95% relative humidity. The concrete specimens are undergoing destructive testing which began in March of 2019.

II. NONDESTRUCTIVE EVALUATION OF CONCRETE SPECIMENS

A linear array ultrasonic tomography instrument, MIRA, was used for the NDE in this research. This version of MIRA incorporates 10 channels, each of which is composed of four transmitting and four receiving dry point contact (DPC) transducers. No contact liquid couple was required for the transmission of horizontal shear waves to the tested medium [3]. The distance between adjacent transducer channels was 40 mm (1.6 in.). This linear array system generated 45 time-of-flight measurements from transmitting and receiving pairs at various distances in less than three seconds.

A rectangular 10 × 10 grid with a 4-inch step in each direction was created on the top surface of each specimen. The measurements were made along each line with a 4-inch step (see Figure 2). Two rounds of testing were conducted on the surface of each test specimen. The first round of testing was conducted on January 20, 2017, and the second round occurred on September 29, 2017. MIRA system parameters were set as follows: center frequency of 50 kHz, impulse duration of 2 half-periods, and one cycle.

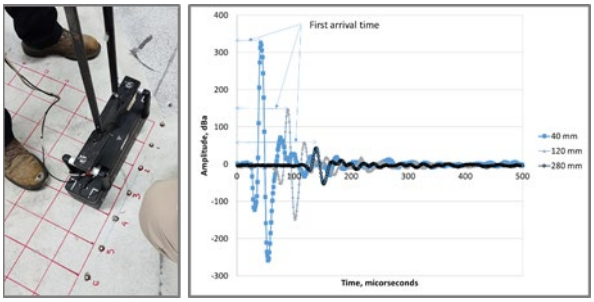

Fig. 2. Ultrasonic NDE measurement on top side of unconfined concrete specimen and example measured signal.

When one of the transducers excites the surface of the slab, the wave propagates through the specimen, and the receiving transducers record the excitations at various locations. This study focused on the analysis of the direct arriving signals: that is, signals resulting from the wave traveling the shortest distance from one transducer to another. In this case, the shortest distance between the transducers is along the surface of the slab, so the signal is mainly affected by the properties of the concrete surface of the specimens. The ASR damage can affect the recorded distance in two possible ways: the presence of the micro-damage may reduce the stiffness of the concrete, resulting in a lower speed of the wave propagation, or microcracks may cause distortion of the shape of the recorded impulse.

II.A. Velocity Analysis

One advantage of the linear array system presented here is that it records signals from pairs of sending and receiving transducers located at various distances. For each signal time history, the arrival time was determined as the time of the maximum value of the arriving signal. Figure 2 shows an example of determination of the arrival time for sensor pairs located 40, 120, and 280 mm apart. A linear regression analysis was performed between arrival times and distances between the sensors for each MIRA measurement. A plot of the distance between transducer pairs and the measured signal arrival time for one of the MIRA measurements is shown in Figure 3. A linear relationship is observed for this data set and the slope of the line, where 2.664 mm/microseconds = 2.664 km/s is the shear wave velocity. A high R^2 of 0.9996 indicates that the model explains 99.96% of the change in the arrival time with the change in the distance between the sensors.

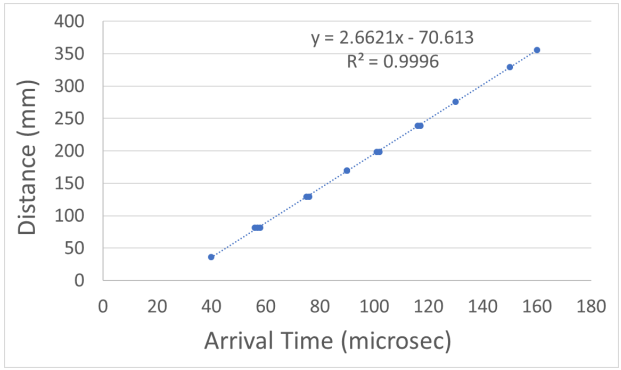

Fig. 3. Shear wave velocity calculation.

If concrete is approximated as an isotropic and elastic medium, then the relationship between elastic parameters (Young's modulus and Poisson's ratio), density, and wave velocity in concrete is shown in Eq. (1) [4],

$$C_s = \sqrt{\frac{E}{2(1+\mu)\rho}}, \quad (1)$$

where E is Young's modulus of elasticity, μ is Poisson's ratio, ρ is density, and C_S is the shear wave (S-wave) velocity. The presence of microcracking reduces Young's modulus of concrete, resulting in reduction of the shear wave velocity.

A full analysis of the data collected on the top surfaces of the confined (CASR), unconfined (UASR), and controlled (CTRL) specimens was completed in the following steps. First, the velocities were computed from each MIRA location measurements. Then the mean and standard deviations were computed for each specimen for the January and September 2017 measurements. Table 1 summarizes the results of velocity analysis. It can be observed that results from both days of testing the shear wave velocities were within the range expected for concrete. However, the velocity of the concrete surface measured on the top of the CTRL specimen was higher than the velocities measured on the UASR and CASR specimens, and this difference is statistically significant. As expected, the velocities for the corresponding specimens increased from January to September. This increase was approximately the same, about 2%, for all three specimens. The standard deviations of the velocities were the lowest for the CTRL specimen, followed by the standard deviations for the CASR specimen, and the standard deviations were the highest for the UASR specimen. The magnitude of the standard deviations increased for all three specimens from January to September.

TABLE I. Shear Wave Velocity for Concrete Specimens

	January 2017 Measurement		September 2017 Measurement	
	Average	Standard Deviation	Average	Standard Deviation
CTRL Top, S2	2.69	0.025	2.739	0.040
UASR Top, S1	2.50	0.037	2.552	0.041
CASR Top, S3	2.47	0.034	2.510	0.039

The presence of damage was not the only parameter affecting concrete shear wave velocity. Other factors, such as elastic properties of the coarse aggregates, as well as concrete mix proportion, also have a pronounced effect. Therefore, the velocity analysis can indicate the presence of the ASR damage only if the velocity of undamaged concrete with the same mix design and aggregate properties is known.

II.B. Analysis of the Shape of the Received Signal

In the past study, the Hilbert Transform Indicator (HTI) was successful in capturing the presence of damage in concrete slabs. Slabs commissioned by the Electric Power Research Institute (EPRI) were made of concrete with properties quite different from those of the large concrete specimens [5]. For example, the shear wave velocity of the undamaged concrete in the EPRI study was about 2.4 km/sec vs 2.7 km/sec in this study. The data collected in this study offered an opportunity to re-appraise potential of the HTI to quantify ASR damage. The Hilbert Transform Indicator (HTI) is defined as follows:

$$HTI = \int_0^{500} \frac{HT(t)}{HT_{max}} dt, \quad (2)$$

where HT(t), the Hilbert transform of a signal f(t), is defined as:

$$HT(t) = \sqrt{\left(f(t)\right)^2 + \left(\frac{1}{\pi}\int_{-\infty}^{\infty} \frac{f(\tau)}{t-\tau} d\tau\right)^2}, \quad (3)$$

where t is time, and HT_{max} is the maximum value of the function HT(t) in the interval from 0–500 microseconds. A time window of 500 microseconds was selected to ensure that the direct arrival impulse, as well as all subsequent oscillations, were captured. A higher HTI value would indicate damaged concrete, while a low value represents sound concrete.

Tables 2 and 3 present the resulting HTI for each specimen from testing conducted in January 2017 and September 2017, respectively. It can be concluded that HTI for the control slab is lower than the HTIs for the specimens with ASR damage. However, the HTI values were significantly lower than those reported for the EPRI slabs: 65–75 for undamaged slabs, and 80–110 for slabs with ASR damage. This suggests that the HTI, which is similar to shear wave velocity, also depends on the undamaged concrete properties. It is hypothesized that adjusting HTI for shear velocity may help to develop an ASR damage indicator applicable to all mix designs. Testing of this hypothesis is a subject of ongoing research.

TABLE II. HTI of January 2017 NDE Measurements

	HTI			
	Average	Standard Deviation	Min	Max
CTRL Top, S2	54.80	2.03	50.30	64.14
UASR Top, S1	58.45	3.37	52.27	70.31
CASR Top, S3	60.72	4.72	50.29	74.08

TABLE III. HTI of September 2017 NDE Measurements

	HTI			
	Average	Standard Deviation	Min	Max
CTRL Top, S2	51.8	1.8	46.8	56.5
UASR Top, S1	58.5	5.0	49.2	109.6
CASR Top, S3	61.5	4.2	53.3	73.4

The signal shape analysis resulted in higher HTI for the ASR specimen than for the control specimen. It confirms findings from the previous studies that an increase in HTI indicates the presence of microdamage near the surface of the concrete structure. However, the HTI values were lower than the those from the previous study. Since the shear wave velocity for the undamaged concrete specimen in this study was significantly higher than the concrete shear wave velocity in the previous study, it was concluded that the HTI should be adjusted for the shear wave velocity to develop a more reliable method for microdamage characterization.

III. IMAGE RECONSTRUCTION TECHNIQUES

The Synthetic Aperture Focusing Technique (SAFT) is a well-known reconstruction technique used for radar and other ultrasonic measurements. SAFT is a cross sectional image of the interior of the medium analyzed using a specialized B-scan, which is a compilation of many A-scans (raw data). It is a delay-and-sum technique that uses time-of-flight signal and the speed of sound in the medium to reconstruct ultrasonic NDE measurements. A

color-based map is created using the signal amplitude between the transmission (Tx) and receiver (Rx) pair. Converting time to distance using the propagation velocity of the material, the round-trip distance is calculated for each Tx-Rx pair.

In previous concrete analysis work, using the Frequency Banded SAFT (FB-SAFT) method [6] and using the wavelet node containing the nominal center frequency of the MIRA has repeatedly shown a reduction in background scatter noise and crisply resolved internal structure and defects [7]. As a longitudinal study of ASR, the repeatability of the positioning of the instrument is paramount. Grids were created on the surfaces using permanent means to ensure that the instrument could be positioned repeatably between collection campaigns. Data were collected using the MIRA instrument from three locations on the CTRL (S2) and UASR (S1) specimens—the top face and the east and west side faces. For the CASR (S3) specimen, data were collected from the top surface only, as this was the only accessible face of the CASR specimen. What follows is one illustrative comparison of the data collected from the UASR specimen in January 2017 and September 2017 along the scanline line-E.

The grid of the UASR block is oriented at a 45-degree angle to the rebar mats of the specimen. Figure 4 shows line-E highlighted and provides context on the rebar orientation with respect to line-E. The horizontal rebars are closest to the surface, and the vertical rebars are below. Data are acquired by progressing along the gridline being scanned and taking an acquisition at each of the intersecting grid lines. As the acquisitions along the scan line are made, redundant data are intentionally acquired, as illustrated in Figure 5.

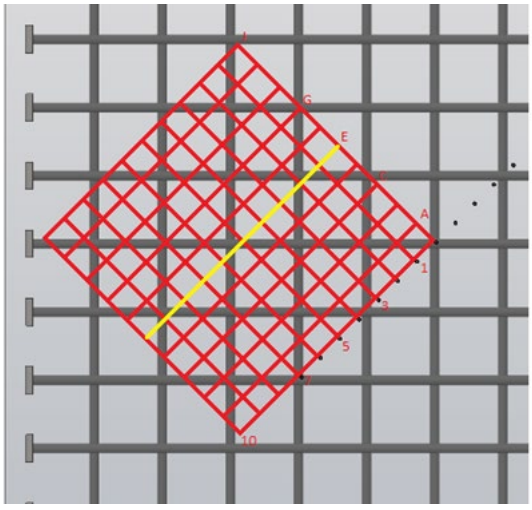

Fig. 4. UASR specimen's top surface showing internal rebar structure, drilled in concrete (DIC) studs, and measurement grid with line-E highlighted in yellow.

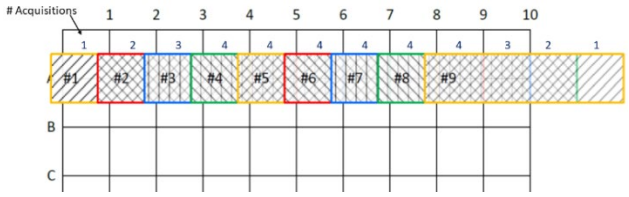

Fig. 5. Illustration of how MIRA is moved horizontally along a gridline, resulting in collection of multiple acquisitions for certain regions.

The FB-SAFT reconstruction containing the nominal center frequency of the MIRA used during the data collections is shown in Figure 6. This is a panoramic composite of nine individual acquisitions made by stepping along line-E and taking an acquisition at the intersection of number grid lines 1 through 9. The lack of "redundant" data samples is clearly visible in the first and last 4 inches in the transverse axis. Figure 4 shows the September data collection from the same target, line-E of the UASR specimen. Figures 6 and 7 use the exact same colormap range to allow one-to-one comparison based on the colormap.

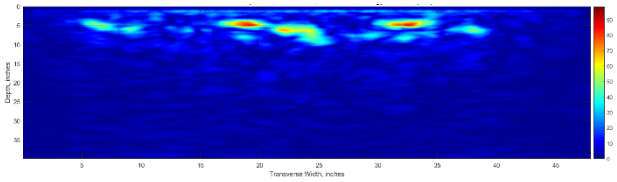
Fig. 6. FB-SAFT panoramic composite along line-E of the UASR January collection using Node-16 (31.25 kHz – 62.5 kHz).

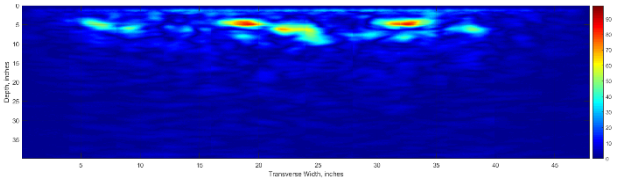
Fig. 7. FB-SAFT panoramic composite along line-E of the UASR September collection using Node-16 (31.25 kHz – 62.5 kHz).

The difference between the two Node-16 FB-SAFT panoramic reconstructions was taken. The absolute value of Hilbert's transformed data produces a rectified envelope of the surface. This is a standard operation, though typically unacknowledged, used on SAFT-generated results. Likewise, to add the identifications of areas with greater differences between the January and September UASR line-E reconstructions, the absolute value of the Hilbert transform of the difference values is displayed in Figure 8.

The point-by-point difference shows a number of areas containing suspected change between the two data

collections. The fact that the majority of the more significant differences are in the top 10 inches is notable and requires further investigation. The specimens are undergoing destructive analysis at the time of this writing, and the resulting data will allow for creation of ground truth information on the specimens. Until then, the analysis of the difference results between the data campaigns shows more differences near the surface. The evaluation of the edges of the collection grid, 0–5 and 43–48 on the transverse width axes, are explicitly ignored in these evaluations, as these regions had single acquisitions and do not benefit from the inherit redundant/duplicate data collection produced by the collection procedure (Figure 5).

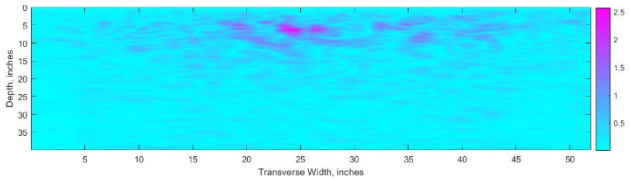

Fig. 8. Absolute value of Hilbert transform of the point-by-point difference between January and September 2017 UASR line-E FB-SAFT reconstructions.

IV. CONCLUSIONS AND FUTURE WORK

In this initial longitudinal study of ASR generation in a controlled environment and in NPP-sized specimens, several previously unconsidered situations were identified. The first noted issue is the repeatability of measurements. As the three specimens are housed in an indoor environmental chamber, the grids are effectively permanent. Therefore, positioning of the MIRA unit was expected to be effectively unchanged between the collection campaigns. However, unanticipated variation in the results comparisons between January and September 2017 data were found in a number of cases around known internal structures, namely, rebar. Given the permanent grid and the fact that the same MIRA unit was used in both data collection campaigns, the unanticipated variation can reasonably be attributed to human factor of manually aligning the alignment marks on the MIRA's body with the grid lines. In considering this human factor, the question is now whether it is reasonable to assume that a human operator can repeatably apply the same amount of pressure to the MIRA's spring-loaded dry-point contact ultrasonic transducers. Subjectively, it seems that a single operator could be capable of applying consistent pressure across a single collection campaign, but it is questionable whether an operator could apply the same pressure across multiple collection campaigns, especially when the campaigns are months apart. Ultimately, the differences are likely minor, even when considering the human in the loop of collecting data with regards to consistent pressure. The differences due to small alignment variations are of greater concern due to the impact this would have on the reliability of one-to-one comparisons of FB-SAFT reconstruction results. Taking the human factor into consideration prevents quantitative, objective declarations on the presence and severity of ASR in the specimens at this time, but once the destructive characterization ground truth is completed, the analysis results can be validated. Secondly, there are indications that for such thick specimens, not enough energy is transitioning from the instrument into and through the block. The lower rebar mats are not visible in the reconstructions at all. Likewise, even though Node-16 contains the nominal center frequency of the ultrasonic impulse, the frequency effects of ASR are unknown.

In conclusion, there are encouraging results that the direct comparison between data collections can be used to evaluate the condition of large concrete structures as they age. Establishing precise positioning and alignment that can be reproduced month after month, year after year will be critical for these types of tests that require the very manual, tedious task of the human operator to position and acquire data. Future work to evaluate the effects of impulse energy and the efficient transfer of energy into a concrete specimen is worthwhile.

REFERENCES

1. Commission, N.R., *Seabrook Station Safety in Light of Alkali-Silica Reaction Occurring in Plant Structures.* 2012.
2. Ezell, N.D.B., et al. *Experimental collaboration for thick concrete structures with alkali-silica reaction*. in *AIP Conference Proceedings*. 2018. AIP Publishing.
3. Shevaldykin, V., A. Samokrutov, and V. Kozlov. *Ultrasonic low-frequency transducers with dry dot contact and their applications for evaluation of concrete structures*. in *2002 IEEE Ultrasonics Symposium, 2002. Proceedings.* 2002. IEEE.
4. Carino, N.J. *The impact-echo method: an overview*. in *Proceedings of the 2001 Structures Congress & Exposition*. 2001. American Society of Civil Engineers.
5. Khazanovich, L., et al. *Nondestructive analysis of alkali-silica reaction damage in concrete slabs using shear waves*. in *AIP Conference Proceedings*. 2018. AIP Publishing.
6. Albright, A. and D. Clayton. *The benefits of using time-frequency analysis with synthetic aperture focusing technique*. in *AIP Conference Proceedings*. 2015. AIP.
7. Clayton, D.A., et al., *Nondestructive evaluation of thick concrete using advanced signal processing techniques*. 2015, Oak Ridge National Lab.(ORNL), Oak Ridge, TN (United States).